Available online at www.sciencedirect.com

SciVerse ScienceDirect

Procedia CIRP 8 (2013) 75 – 80

www.elsevier.com/locate/procedia

14th CIRP Conference on Modeling of Machining Operations (CIRP CMMO)

3D Simulation and Process Optimization of Laser Assisted Milling of Ti6Al4V

Hassan Zamani[a*], Jan-Patrick Hermani[b], Bernhard Sonderegger[a], Christof Sommitsch[a]

[a]*Institute for Materials Science and Welding, Graz University of Technology, Kopernikusgasse 24/I, Graz 8010, Austria*
[b]*Fraunhofer Institute for Production Technology IPT, Steinbachstrasse 17, 52074 Aachen, Germany*
* Corresponding author. Tel.: +43 -316- 873 - 1678; fax: +43-316-873-7187.*E-mail address*: hassan.zamani@tugraz.at.

Abstract

Recently, the high cost and low productivity of machining hard materials such as Ti-6Al-4V has drawn major attention to the development of a modular and scalable tool system with integrated laser as one piece of equipment. The present study focuses on a new concept of laser-assisted milling with spindle and tool integrated laser beam guiding. The laser beam is located at the cutting area and moving synchronously with the cutter. In order to optimize the process with respect to the force reduction, various machining conditions were investigated, both experimentally and with simulation. The numerical 3D FEM simulations were carried out with the commercial software DEFORM 3D. In the simulation, a Johnson-Cook type material model was applied and specifically modified for very high strain rates and system temperature. Results such as temperature distributions and maximum cutting forces could directly be compared to the experimental findings. The simulation results expressed a good agreement with the experimental results.

Selection and peer-review under responsibility of The International Scientific Committee of the "14th CIRP Conference on Modeling of Machining Operations" in the person of the Conference Chair Prof. Luca Settineri

Keywords: Type your keywords here, separated by semicolons ;

1. Introduction

Although laser assisted machining is known for a long time and has been studied for a wide variety of high strength materials such as Ni-, Ti- or Co-base alloys or technical ceramics, e.g. silicon nitride (Si_3N_4) [1,2], the application of LAM in machining of hard-to-machine materials is not routine in industry. Today, the availability of more cost-effective laser sources provide a new challenge to develop a modular and scalable tool system with integrated optics in terms of equipment without any additional peripheral device as it is realized by Fraunhofer IPT [3]. Along with practical efforts, a thermo-mechanical process model for laser assisted machining of high strength metallic and ceramic materials reduces time consuming testing periods. In this work, a finite element model for the corresponding process was set up to predict required process parameters for different materials, operation modes and components geometries. Based on nonlinear thermal softening at high strain rates a new aspect in applying of Johnson-Cook material model for Ti-6Al-4V alloy was considered. The model was adapted using several cutting force measurements in different cutting conditions.

2. Experimental and Numerical Procedures

2.1. Experimental procedures

Laser-assisted milling experiments were carried out on a Satisloh G1 3+2 axis machining center with Bosch Rexroth MTX P60 NC control. Fig. 1 gives an overview of the spindle-tool sys-tem with integrated optical and mechanical interfaces. Optical system components such as safety glasses, lenses, brass tubes and fixtures are integrated into an optical module of a considerably large HSK-100 C milling system. In order to prevent the optical lens and mechanical components from the overheating, the process gas is supplied over a rotary lead through interface on the spindle housing which is

2212-8271
Selection and peer-review under responsibility of The International Scientific Committee of the "14th CIRP Conference on Modeling of Machining Operations" in the person of the Conference Chair Prof. Luca Settineri
doi:10.1016/j.procir.2013.06.068

tied to collimating lens. Furthermore, the process gas pushes away the dispersed chips from the optical lens and the beam path, which supports the thermal process efficiency. An IPG YLR high fiber laser (Yb: YAG with a wavelength of 1070 mm) with a peak power output of 6 KW via light conducting cable, was applied to the laser radiation. The diverging laser beam is changed into a nearly parallel beam by an aspheric collimating lens and transports through the spindle with hollow shaft. A tool integrated focusing system converts the delivered beam into the converging laser beam. Two hr-coated mirrors reflect the laser beam directly on the cutting surface edge in front of the cutting insert. The laser power is switched on/off at entrance and exit points, receptively and a camera-based monitoring system controls the workspace area whether it is completely closed during laser-assisted machining. The laser power is modified according to the uncut chip thickness during one revolution in the milling process. The machining mode was set up for the side milling. All the experiments were performed with round inserts (RDHX 07 07 MOT D*D1*S- 7*2.7*2.38 with the rake angle 11°) at a fixed depth of cut of 0.5 mm using TiAlN-coated cemented car-bide. The maximum laser power varied from 0 to 1758 W, while the laser spot diameter was 1 mm. The fixed distance between insert and the center of laser spot (arc length) is 5 mm. The machining tests were conducted at different cutting velocity and feed rate with a mill diameter of 24 mm and a cutting width of 8 mm. The workpiece material was forged Ti-6Al-4V in annealed, pickled and stress relieved condition. A piezo-based three dimensional force measurement determined the process forces in 3 directions (the coordinate system is shown in Fig.1 the feed direction is along the X axis) during the machining experiments. For one path of milling, the maximum forces in each revolution (with the frequency of 200 up to 450 kHz) were aver-aged. The forces were saved automatically with program based on NI LabVIEW.

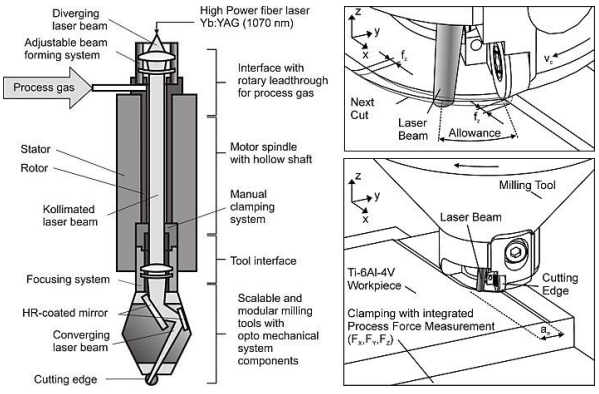

Figure 1: The working principle of the novel laser-assisted-milling [3].

The average absorptivity of Ti6Al4V passing an Yb: YAG laser with a wavelength of 1070 nm is about 0.4, but this value can vary with laser parameters and surface roughness, defects and impurities, thin films and oxidation layer. In or-der to find the absorbed portion of laser energy in the according process, based on the metallographic analysis (because of high cutting velocity, the inline temperature measurement presented a poor accuracy) tried to estimate the surface temperature. For this purpose, first, the machining was carried out to prepare surface condition, then, the workpiece was irradiated only once without tool engagement. Fig. 2 shows a metallographic result of the achieved surface at a cutting velocity of 25 m/min for different laser power. Depending on surface temperature and cooling rate (air cooling rate), different microstructures were obtained: (I) initial microstructure (α+β), (II) no martensitic trans-formation but β transformation from α, (III) partial martensitic transformation, (IV) complete martensitic transformation, (V) oxide layer and white surface layer (as a result of surface melting). The ratio of each domain and also occurrence of white surface layer characterize a certain temperature range. Based on metallographic studies accompanied with numerical simulation, the absorption coefficient for Ti6Al4V alloy in this process was determined about 0.27 ± 0.03.

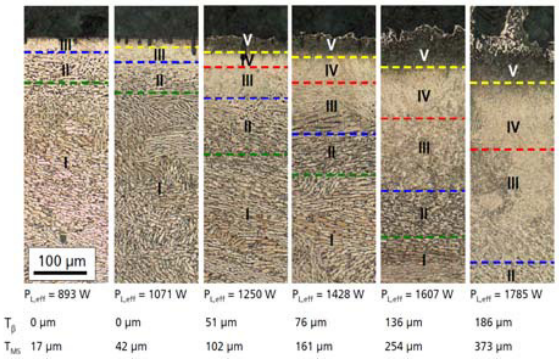

Fig. 2: Metallographic analysis of microstructure change with the different laser power at a constant cooling rate.

2.2. FE-numerical procedures

The commercial software DEFORM 3D has been used to set up a thermo-mechanical FEM model for the laser-assisted machining process (Fig. 3). The implicit Lagrange mesh formulation is able to handle large deformations, but requires frequent remeshing. The software supports automatic local remeshing, based on the impacted weighting factors. In regions with high strain, strain rate and temperature, the generated mesh is finer (in the primary shear zone and the area near the tool tip) [4]. The model represents the workpiece as a

rigid-plastic part and the tool as a rigid body with tetrahedral elements for both. The thermal boundary conditions (convection and radiation) were considered by applying the convection heat transfer coefficients and the emissivity to all elements with external contact. Tool movement was defined as rotation around the vertical axes and constant velocity in the feed direction, while the coordinate system (mill center) moves according to the tool. The bottom surface of the workpiece was fixed in three directions. Based on the Zorev's model [5], the tool-chip contact area is divided into two regions according to the stress state on the rake face; sticking, governed by high normal stress, and otherwise sliding. Therefore, the tangential shear stresses on the tool surface cannot exceed the yield shear stress of chip material. The following relations express the frictional condition at the tool-chip interface:

$$\begin{aligned} \tau &= \mu\sigma_n, \quad \text{if} \quad \mu\sigma_n < \bar{m}\frac{\sigma_{eq}}{\sqrt{3}} \\ \tau &= \bar{m}\frac{\sigma_{eq}}{\sqrt{3}}, \quad \text{if} \quad \mu\sigma_n \geq \bar{m}\frac{\sigma_{eq}}{\sqrt{3}} \end{aligned} \tag{1}$$

where σ_n is the normal stress, τ is the shear stress, σ_{eq} is the equivalent flow stress, μ is Coulomb friction coefficient and $\bar{m}$ is the shear factor. The value for $\bar{m}$ and μ were kept constant at 0.7 and 0.5, respectively. The heat interface coefficient between tool and chip is taken as a constant value of 50 kW/m²K.

Furthermore, the effect of process gas was considered by defining a heat transfer coefficient as the forced convection of 2000 W/m²K.

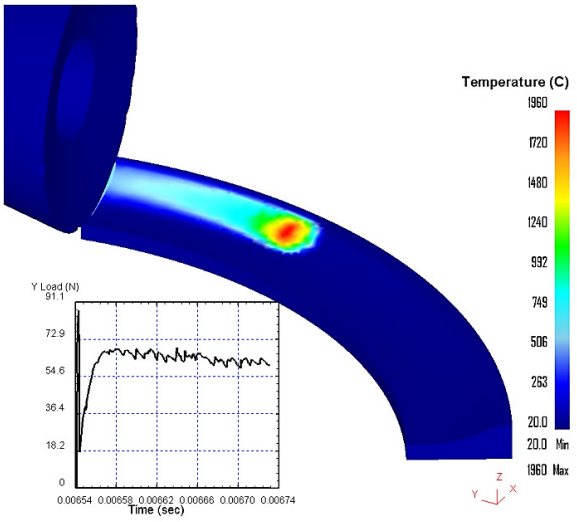

Fig. 3: 3D FE-model of laser-assisted-side milling process.

The Johnson-cook constitutive material model is used widely to calculate material's flow stress in FE simulation of machining processes.

$$\sigma_{eq} = (A + B\varepsilon^n)\left(1 + C\ln\left(\frac{\dot{\varepsilon}}{\dot{\varepsilon}_0}\right)\right)\left(1 - \left(\frac{T - T_r}{T_m - T_r}\right)^m\right) \tag{2}$$

where σ_{eq} is the equivalent flow stress, ε is the equivalent plastic strain, $\dot{\varepsilon}$ is the equivalent plastic strain rate normalized by a reference strain rate $\dot{\varepsilon}_0$, T_m is the melting temperature of the material and T_r is the room temperature, while A, B, C, n and m are material constants. Lee and Lin [6] determined these constants for strain values up to 0.35, strain rate up to 3300 s^{-1} and temperatures up to 1100°C. Unfortunately, one of the deficiencies of this flow law is the constant thermal softening rate up to the melting temperature, which makes it unsuitable for modeling localization and instability problems.

Table 1. Material constants

Constants	Values
A (MPa)	724
B (MPa)	683.2
C	0.035
m	1.0
n	0.47
T_m (°C)	1660
a	10^{-7}
b	2.9
m_0	1
$\dot{\alpha}$	10^{-4}

With the assumption that in sufficiently high strain rate domains, the generated heat due to the deformation does not have sufficient time to dissipate, H. Frost and M. Ashby [7] introduced a simple way to find the minimum strain rate ($\dot{\varepsilon}_c$) for occurrence of adiabatic shear:

$$\dot{\varepsilon}_c = \frac{-\dot{\alpha}nk(T)}{R^2\left(\partial\sigma/\partial T\right)_{\varepsilon,\dot{\varepsilon}}} \tag{3}$$

where $\dot{\alpha}$ is a constant, n is the strain hardening, k the thermal conductivity and R a characteristic length scale. Fig. 4 shows a 3D chip formation and strain localization with an assumption that flow stress decreases by a factor of 10 as the strain rate reaches the critical value. The model reacts to each cutting velocity and temperature in terms of tooth depth and spacing.

In order to consider the effect of localized deformation for large scale simulations, the rate of thermal softening should be accelerated at areas with high strain rates which can be determined with Equation (3) by replacing the minimum element size instead of R. Hence, in this work, as the strain rate exceeds the critical strain rate, the thermal softening coefficient (m) in the Johnson-Cook material model behaves as:

$$m = m_0 \exp(-aT^b) \quad (4)$$

where a and b are constants and m_0 is the initial thermal softening coefficient. All constants are listed in Table 1. The subroutine describing the nonlinear thermal softening at the regions exceeding the macro-scale critical strain rate was successfully implemented into the 3D FE-model for the cutting simulation.

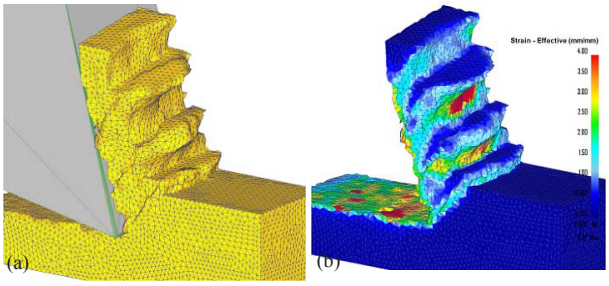

Fig. 4: (a) 3D chip segmentation of machining of Ti-6Al-4V at a cutting velocity 90 m/min and (b) localized effective strain distribution in the direction of maximum shear stress.

A 3D moving laser heat source model (Fig. 5-a) was developed to predict the temperature distribution including the impact of the laser beam. The model considers natural boundary conditions and temperature depending thermo-physical material properties (which are taken from Mill [8]).

The laser spot reaches a steady of the temperature as the laser moves along its diameter, depending on the absorbed laser power density. Since temperature calculation and mechanical simulation run in parallel, cutting forces can be determined depending on the input laser power. Within each time step, the absorbed power (P) per unit area A can be defined, introducing a virtual environmental temperature T_e which represents the laser power:

$$P = Ah(T_e - T_s) \quad (5)$$

If the local convection coefficient (h) approaches zero, T_e gets significantly higher than the surface temperature (T_s), which leads to:

$$T_e - T_s = \frac{I}{h} \cong T_e \quad (6)$$

Thus, in the surface region of direct laser input, the virtual environmental temperature can be calculated directly out of the laser power density (I), ($I = P/A$) divided by a very small value of the convection coefficient (e.g. 0.0001).

This model enables to investigate the effect of laser power, laser spot size, and distance between insert and laser spot incident angle, rotation velocity and feed velocity on the resulting temperature field. Also, it is possible to vary the laser power during one revolution of the mill according to the chip thickness. As shown in Fig. 5-b, 5-c and 5-d laser power and maximum temperature at the laser spot decreases linearly in a rotation.

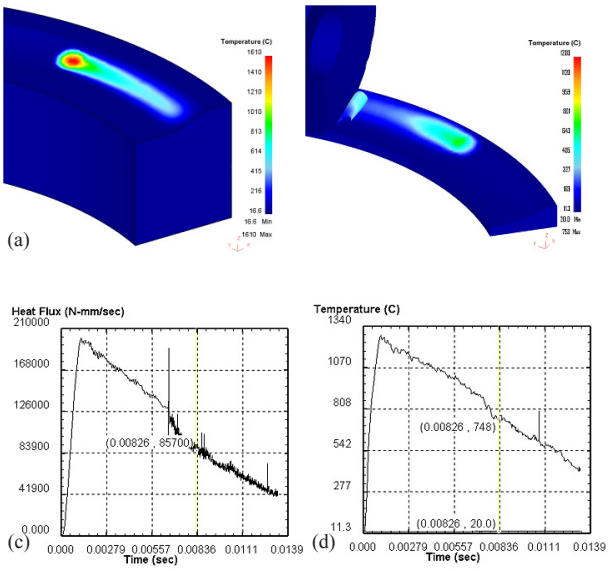

Fig. 1: (a) 3D rotating laser heat source (Laser power with Gaussian distribution: 1000 W, angular velocity: 70 rad/s, feed velocity: 0.77 mm/s) (b) integrated laser heat source with machining process (time dependent laser power) (c) laser power variation during one revolution (d) maximum temperature at the laser spot.

3. Results and Discussion

3.1. Experimental results

Result of experimental trials show generally a reduction in three components of forces in all cutting conditions as illustrated in Fig 6.The reduction of the main cutting force in Y direction decreases gradually with laser input down to a power of approximately 600-800W. The vertical force component (FZ) generally decreases at low laser power (lower than 1428 W) between 1428-1758W, the force reduction is not clear due to a number of uncertain aspects in the experiment. The reasons can be justified by adhesive bonding of the chip on the tool tip as the laser power increases especially at low speed machining and low feed rate. This phenomenon increases the contact area and stress state in the vertical direction leading to unexpected results. Anyway, the reduction of Z forces as a function of material removal rate is of more interest, because this force component increases rapidly in conventional

machining with machining time in comparison with the LAM [9].The largest reduction between the conventional and LAM can be observed for a cutting velocity 25 of m/min and a feed rate 90 of µm/rev, although variations get small at laser powers higher than 1428 W. With increasing feed rate, the forces increases but the absolute amount of reduction in forces does only change slightly.

In this process, increasing the laser advance more than 5 mm shows a negative effect on the amount of reduction.

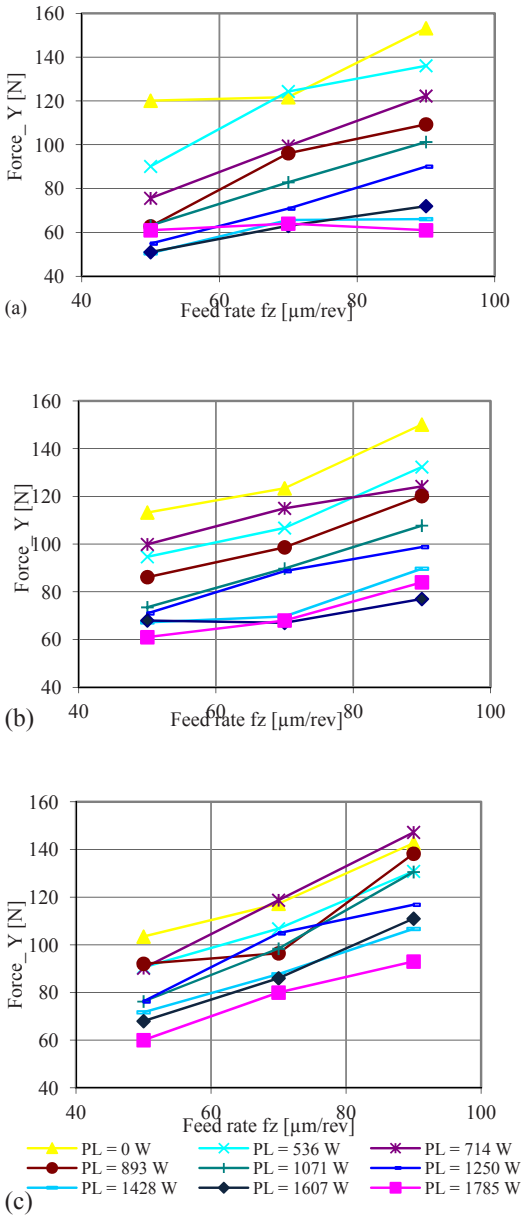

Fig. 2: The variation of the main cutting force F_Y with the laser power, (a) cutting velocity of 25 m/min, (b) 50 m/min and (c) 100 m/min.

3.2. Numerical simulation results

In order to validate the model, developed in the present work, the numerically calculated cutting forces were compared to the experimentally determined ones. With the purpose of process optimization, the model was verified for different cutting conditions such as cutting velocity, feed rate and laser power. The forces reported in the histograms of Fig. 7 were obtained as maximum values of the load signals (as shown in Fig. 3) before the simulation approaches the steady state for further calculations such as temperature and wear.

For comparison, a TANH material model [9, 10] was applied in this study to state the difference between the two models. As is observed in Fig. 7, the non-linear thermal softening at high strain rates provides a wide range of validity for the simulation results. Contrary to this model, the TANH material model produces lower forces in case of machining without laser and is not capable to predict the force reduction with varying in laser power fairly.

An excellent agreement for cutting forces in Y-direction was found for the used model. The forces in Z-direction showed a very good agreement for laser powers up to 1428W. The amount of predicted force reduction with in-creasing the laser power in X direction is higher than the experimental results.

The simulation results validate that the developed thermo-mechanical FEM model for the laser-assisted machining in the tested cutting conditions is robust and can be utilized for process optimization. Because of the large element size used in the simulations (minimum element size was 0.015 mm in the primary shear zone) the chip morphology in this process was not considered.

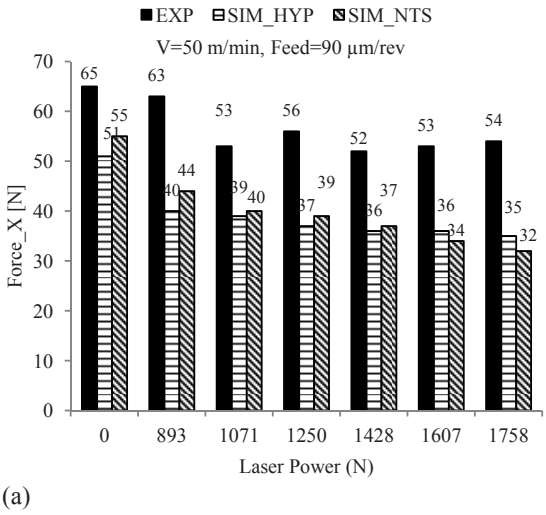

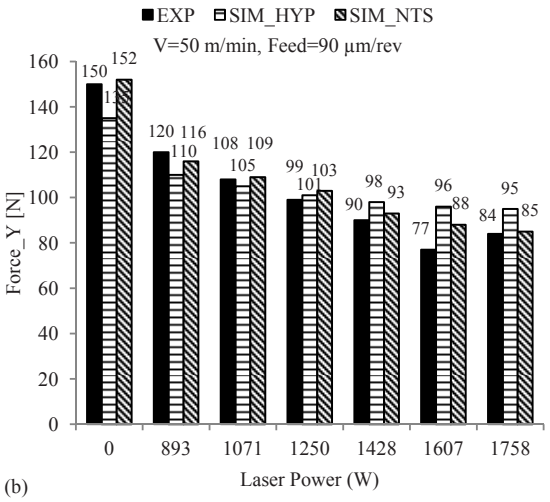

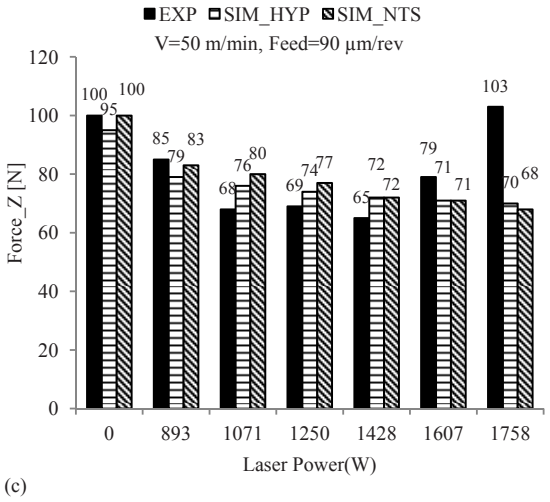

Fig. 3: Comparison between simulated and measured milling forces with increasing laser power for used-JC-model (NTS) and TANH model (HYP).

4. Conclusion

The results of laser-assisted milling of Ti-6Al-4V using TiAlN-coated cemented carbide cutting insert in different cutting conditions has been presented. A significant reduction of forces was achieved by the optimization of both machining and laser parameters. The results showed a reduction of force in X-direction up to 25%, Y-direction up to 60% and Z-direction up to 65%. Furthermore, the tool wear could be reduced significantly by the assistance of the laser, resulting in an increased tool life. Beside the experimental investigations, the effects of varying process parameters were studied within a 3D-FEM simulation. A nonlinear thermal softening coefficient was applied to state the thermo-mechanical behaviour of Ti-6Al-4V in the according process. This modification was based on the acceleration of thermal softening in areas with the critical strain rates where time is not sufficient for significant heat dissipation from the primary shear zone. The results showed very good agreement between simulated and experimentally found cutting forces.

Acknowledgements

The research work presented in this paper is part of the TooLAM project, funded by the European Union and the Austrian Research Promotion Agency (FFG) within the EraSME program.

References

[1]. W. König, A. Zaboklicki, 1993, Laserunterstützte Drehbearbeitung von Silizium-Nitrid-Keramik, VDI-Z 135/6, p. 34-39.
[2]. E. O. Ezugwu, Z. M. Wang, 1997, Titanium alloys and their machinability—a review, Journal of Materials Processing Technology, 68, p. 262–274.
[3]. C. Brecher, M. Emonts, C. J. Rosen and J. P. Hermani, 2011, Laser-assisted Milling of Advanced Materials, Physics Procedia, 12: 599-606.
[4]. Deform-User Manual SFTC-Deform V10.0.2, 2010, Columbus (OH), USA.
[5]. N. Zorev, 1963, Inter-relationship between shear processes occurring along tool face and shear plane in metal cutting, International Research in Production Engineering, p. 42-49.
[6]. W.S. Lee, C. F. Lin, 1998, Plastic deformation and fracture behavior of Ti6Al4V alloy loaded with high strain rate under various temperatures, Materials Science and Engineering, A241, p. 48–59.
[7]. H. J. Frost, M. F. Ashby, 1982, Deformation mechanism maps, Pergamon Press, Oxford.
[8]. K. C. Mills, 2002, Recommended Values of Thermo physical Properties for Selected Commercial Alloys, Woodhead Publishing, 217.
[9]. M. Sima, T. Özel, 2010, Modified material constitutive models for serrated chip formation simulations and experimental validation in machining of titanium alloy Ti6Al4V, International Journal of Machine Tools and Manufacture 50, p. 943-960.
[10]. H. Zamani, J. P. Hermani, B. Sonderegger, C. Sommitsch, 2013, 3D Simulation of Laser Assisted Side Milling of Ti6Al4V Alloy using Modified Johnson-Cook Material Model, 16th annual ESAFORM Conference on Material Forming, in press.